Enkovaara, J.; Nordström, Lars; Nieminen, R.M

Magnetic anisotropy in Ni2MnGa

Published in:
Physical Review B

DOI:
10.1103/PhysRevB.65.134422

Published: 01/01/2002

Document Version
Publisher's PDF, also known as Version of record

Please cite the original version:
Enkovaara, J., Nordström, L., & Nieminen, R. M. (2002). Magnetic anisotropy in Ni2MnGa. *Physical Review B*, *65*(13), 1-7. [134422]. https://doi.org/10.1103/PhysRevB.65.134422

Magnetic anisotropy in Ni_2MnGa

J. Enkovaara* and A. Ayuela
Laboratory of Physics, Helsinki University of Technology, P.O. Box 1100, FIN-02015 HUT, Finland

L. Nordström
Department of Physics, Uppsala University, P.O. Box 530, SE-751 21 Uppsala, Sweden

R. M. Nieminen
Laboratory of Physics, Helsinki University of Technology, P.O. Box 1100, FIN-02015 HUT, Finland

(Received 5 July 2001; published 19 March 2002)

We study here, within the density-functional theory, the magnetic anisotropy energy (MAE) in Ni_2MnGa which is a prototype of a magnetic shape-memory alloy. We calculate the MAE, which is a key property for the magnetic shape-memory effect, for tetragonal structure with different ratios of the *c* and *a* lattice constants, reproducing the experimental easy axes both in compression and elongation of the structure. Good agreement between the theory and the experiments in the actual values of the MAE is also found when the nonstoichiometry of the experimental samples is modeled with a simple rigid band approximation. In addition, we estimate the magnetostriction coefficient, confirming the difference between the ordinary magnetostriction and the magnetic shape-memory effect. Equally important, we study the microscopic origin of the MAE in Ni_2MnGa with the spin density and the orbital moment anisotropy and extend the analysis of the orbital moment anisotropy to the ternary compounds. These results show that the largest contribution to the MAE comes from Ni, in spite of the larger magnetic moment in the Mn sites.

DOI: 10.1103/PhysRevB.65.134422 PACS number(s): 75.30.Gw

I. INTRODUCTION

Novel materials which can function as sensors as well as actuators are attaining increasing interest from a technological point of view. In this context, magnetic shape-memory (MSM) alloys[1] are promising. The magnetic control offers fast response compared to the temperature-driven conventional shape-memory alloys,[2] and in addition, strains are larger than in the ordinary magnetostrictive materials.[3] In fact, unusually large strains up to 6% under a magnetic field have been observed in recently developed Ni-Mn-Ga alloys close to the stoichiometric composition Ni_2MnGa.[4] The MSM effect, which differs from the ordinary magnetostriction also by its mechanism, is driven by the magnetic anisotropy energy (MAE). The purpose of this paper is to study the MAE and its origins in the prototype MSM alloy Ni_2MnGa with first-principles calculations.

The MSM effect is based on the magnetic-field-induced redistribution of twin variants in the martensitic phase.[5] When Ni_2MnGa alloy is cooled down, it undergoes a structural transformation from a cubic (austenitic phase) to a tetragonal structure (martensitic phase). In the cubic structure there are three crystallographically equivalent directions for the tetragonal deformation. Therefore, the martensitic phase consists of regions which have different deformation directions. These regions are called twin variants and they are separated by well-defined boundaries. Naturally, the local crystallographic structure determines the easy axis of magnetization, so that different variants have a different global direction for the easy axes i.e., the local magnetic moments in the different variants have different directions in the absence of an external magnetic field. Now, when an external magnetic field is applied to the sample, the local magnetizations try to align with the external field. For fields below saturation and with a large enough MAE, it will be energetically favorable to redistribute the twin variants: instead of rotating the magnetizations with respect to their local crystal structure, the twin boundaries move and the easy axes align with the field. On the whole, this movement leads to the large shape changes observed in the MSM alloys. Although the MSM mechanism differs from ordinary magnetostriction, the magnetostriction coefficient remains still a basic property in the MSM materials. The crucial magnetic parameter is, however, the MAE.

Apart from a large MAE, the MSM effect requires of course the occurrence of both ferromagnetism and a martensitic phase transformation. The martensitic transformation in Ni_2MnGa involves tetragonal distortions from the cubic $L2_1$ structure shown in Fig. 1. Both phases are ferromagnetic

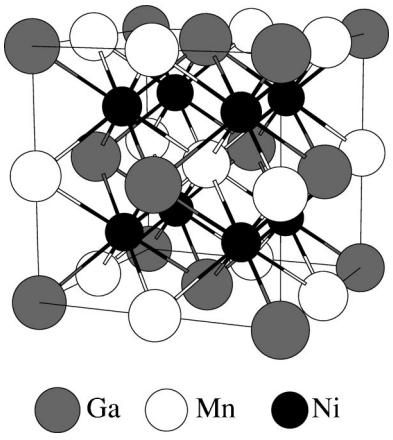

FIG. 1. The $L2_1$ structure.

with the magnetic moment mainly on the Mn sites. These have been studied experimentally with x-ray and neutron diffraction[6,7] and with theoretical calculations.[8] While magnetization curve measurements[9–12] showed that the martensitic phase of Ni_2MnGa has uniaxial magnetic anisotropy, the microscopic origins of the MAE in this alloy have not been studied. Our purpose is to investigate the role of the constituent atoms for the MAE and to sketch the composition dependence of the MAE around the Ni_2MnGa stoichiometry.

The two main sources of the MAE are the spin-orbit coupling and the magnetic dipole-dipole interactions. The dipole-dipole induced anisotropy depends on the shape of the sample and in many cases it is small compared to the spin-orbit coupling.[13] The spin-orbit interaction $H_{so}=\xi \mathbf{L}\cdot\mathbf{S}$, which has a relativistic origin, couples the spins to the underlying crystal lattice, giving rise to an anisotropy.

As a ground-state property, the MAE can be calculated via the density-functional theory. However, the smallness of the MAE makes the calculation difficult. In transition metals, the spin-orbit coupling strength ξ is typically about 50 meV and the MAE, as a fourth-order effect in the cubic symmetry, is therefore of order of μeV. Calculations within the density functional theory have produced relatively good values for Co and Fe,[14] but for Ni even the correct easy axis is not reproduced. In surfaces and in systems with a lower symmetry the MAE is a second-order effect, making the calculations more tractable.[15–17] Up to now, calculations have been performed mostly for monoatomic or binary compounds. We present here calculations for a ternary compound.

A deeper understanding of the physics behind the magnetic anisotropy is brought about by the connection between the MAE and the anisotropy in the orbital magnetic moment. In the absence of the spin-orbit coupling the orbital moment is largely quenched by the crystal field. The spin-orbit coupling induces some orbital moment, which in tetragonal structures can be further enhanced due to a lowered symmetry. Due to spin-orbit coupling, there is orbital moment anisotropy (OMA) which was shown to be proportional to the MAE in the cases with a single atom in the unit cell, assuming that the majority band is completely filled and spin-flip terms are neglected.[18] As the spin-flip terms and contributions from the other spin subband can be important, this relation was generalized, showing that in addition to the orbital moments, the MAE contains contributions also from a magnetic dipole term.[19] However, little research has been done on the interpretation of this relation for compounds with several atoms. The connection between the MAE and the OMA has been formulated for these cases in Ref. 20 and we present here the analysis for a ternary compound.

The calculations in this work are done using the full-potential linearized augmented plane-wave (FLAPW) method[21] and the main aspects of the scheme are described in Sec. II. Since the MSM effect takes place in the tetragonal structure, we calculate the MAE for different tetragonal geometries in Sec. III A. We also discuss the composition dependence of the MAE in terms of a simple rigid band model and determine the magnetostriction coefficient from the calculated MAE. Furthermore, we investigate the microscopic origins of the MAE in Sec. III B with the spin density and the OMA, where we extend the analysis of the relationship between the MAE and the OMA to the tetragonal distortions of this ternary alloy. Finally, we draw the conclusions in Sec. IV.

II. COMPUTATIONAL DETAILS

A. Method

The calculations are done within the density-functional theory using the FLAPW method as implemented in Ref. 22. The generalized gradient approximation[23](GGA) is used for the exchange and correlation potentials. The spin-orbit coupling is treated within the second-order variational method.[24] The plane-wave cut-off for the scalar relativistic basis functions is $R_{MT}K_{max}=9$, leading to $\sim$350 plane waves with the smallest muffin-tin radius $R_{MT}=2.2$ a.u. In the second variational step states up to 3.5 Ry are included in the basis. Since the spin-orbit coupling is a local effect, it is included only within the muffin-tin spheres. The sphere radii used are 2.4, 2.3, and 2.2 a.u. for Ga, Mn, and Ni, respectively. Only the spherical part of the potential is used when calculating the spin-orbit matrix elements. The effects of increasing the sphere radii or the energy cutoff for the second variational step were checked, neither of them changing the results.

The MAE can be calculated as a difference in the total energy between the different magnetization directions. This requires subtraction of two large numbers in order to obtain one small number, and the total energy calculations must therefore be converged extremely well. However, the fact that the spin-orbit coupling is a small effect can be used to simplify the calculation of the MAE. According to the force theorem[25,26] the energy difference ΔE associated with the MAE can be calculated as a difference in the band energies,

$$\Delta E=\sum_i e_{[110]}-\sum_i e_{[001]}. \tag{1}$$

The eigenvalues e_i are determined in the second variational step, the subscripts [110] and [001] refer to the magnetization direction, and the summation is over bands and $\mathbf{k}$ points. The calculations are simplified considerably since only one self-consistent scalar relativistic calculation is needed. The convergence of the self-consistent calculation is also not so crucial as when determining the MAE from total energies. The validity of the force theorem is checked in the next subsection.

The presence of spin-orbit coupling together with spin polarization leads to a lowering of symmetry. Only the symmetry operations of the scalar relativistic system which leave the spin quantization axis invariant remain when the spin-orbit coupling is included. In the tetragonal structure with the [001] magnetization the symmetry is not lowered, but when the magnetization is rotated to the [110] direction only 8 symmetry operations from 16 remain. First, the scalar relativistic potential is calculated with the full (not lowered by spin-orbit coupling) symmetry. Second, the scalar relativistic wave functions and the spin-orbit Hamiltonian are calculated in a $\mathbf{k}$ mesh in the first Brillouin zone, which is obtained using only the 8 symmetry operations which are common for

both spin quantization axes. In this way only one set of scalar relativistic wave functions is needed.

B. Brillouin zone integrations

Within the force theorem, the MAE is determined solely from band energies. Therefore, the Brillouin zone integration is the dominant source of errors. As the MAE is a small quantity and sensitive to the exact structure of the Fermi surface, a very dense mesh of **k** points is needed. Different integration schemes have been used in the literature in order to reduce the number of **k** points. A possibility is to use some broadening technique, such as Gaussian[27] or Fermi[28] broadening, to smooth out the discontinuities at the Fermi level. The problem is that the size of the appropriate broadening is not known in advance: small broadening does not improve the convergence, while too large broadening will affect the results because these methods do averages over the Fermi surface. Another technique for the Brillouin zone integrations is provided by interpolation methods such as the linear tetrahedron method[29] and its modified version.[30] The tetrahedron method is free of adjustable parameters and it should converge to the correct result in the limit of infinitely dense **k** mesh. However, the problem in the tetrahedron method is that band crossings are not taken into account; i.e., the ordering of bands can be incorrect and errors arise when the band crossings occur near the Fermi level. In this section we test the convergence of some integration methods in the calculation of the MAE.

We use the tetragonal structure corresponding to the experimental one ($c/a=0.94$). The self-consistent scalar relativistic calculation is done using the modified tetrahedron method with 8000 **k** points in the full Brillouin zone. The eigenvalue sums of Eq. (1) are then calculated with different **k** meshes and integration methods. All the subsequent MAE values are given with respect to a formula unit. As shown in Fig. 2, the Fermi broadening improves the convergence of the corresponding MAE's when increasing the width of the broadening. However, the results also change and the MAE which is obtained with large broadening is not necessarily correct. Although the results with a small broadening agree with those of the tetrahedron method, the convergence is slower. Since the convergence behavior is not improved from that of the tetrahedron method, there is no benefit using the Fermi broadening method. We have therefore used the tetrahedron method with 33000 **k** points, which gives a good convergence, in all the following calculations.

Some total energy calculations are also performed to check the validity of the force theorem. As also shown in Fig. 2, the difference between the values obtained with the force theorem and with the total energies is small so that the use of the force theorem is justified.

III. RESULTS AND DISCUSSION

A. MAE and magnetostriction

The MAE is calculated for different tetragonal structures while keeping the volume fixed to the theoretical volume of the cubic structure.[8] The calculated MAE as a function of the tetragonal distortion is shown in Fig. 3. The values of the MAE in tetragonal structures are about two orders of magnitude larger than in the cubic structure, as is expected due to a lower symmetry. Within the scope of this work the MAE in the cubic structure is considered to be zero. In the tetragonal structures (see Fig. 3) the [001] axis changes from easy to hard when c/a goes through 1. These calculations reproduce the experimental easy axis both for $c/a<1$ (Refs. 9–11) and for $c/a>1$ (Ref. 31), but the theoretical value is about 2.5-3.5 times higher compared with the experimental values 50-74 μeV for $c/a=0.94$.

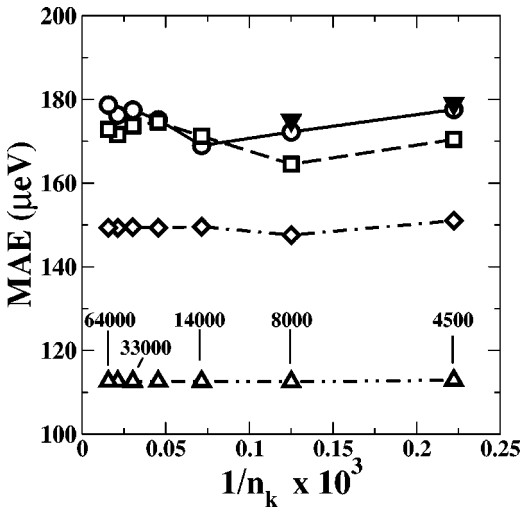

FIG. 2. The MAE as a function of the inverse of the number of **k** points. Some corresponding numbers of **k** points, n_k, in the full Brillouin zone are also shown in the figure. (○) tetrahedron method; Fermi broadening of (□) 27meV, (◇)68 meV, and (△)136 meV; (▼) self-consistent. Lines are only guides for the eyes.

There are at least two important differences in the experiments and in the theory which can explain the discrepancy in the value of MAE. First, the measurements are done at room temperature, while our calculations refer to zero temperature. The overall temperature dependence of MAE is complex as it includes effects from electronic states, magnons, and

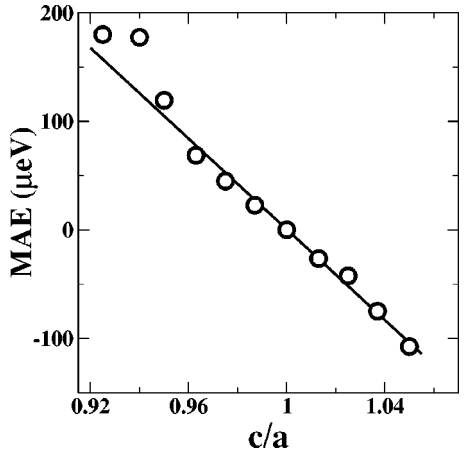

FIG. 3. The MAE as a function of the tetragonal distortion. The solid line is a fit to the linear part of the curve, $c/a>0.96$.

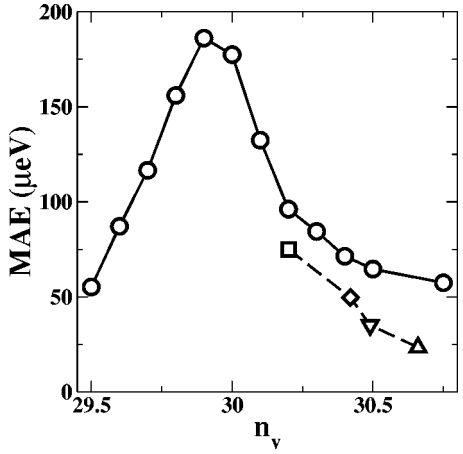

FIG. 4. The MAE as a function of the number of valence electrons per formula unit, n_v, for $c/a=0.94$. Experimental values: (□) Ref. 9, (◇) Ref. 11,(∇) Ref. 12, and (△) Ref. 10.

phonons. The electronic contribution can be obtained from the calculations with the Fermi broadening, Sec. II B, which suggest that in Ni_2MnGa the MAE increases with decreasing temperature, althought one should remember that the temperatures in Fig. 2 are very high. This trend is in agreement with the case of tetragonal Ni,[15] while for Ni_2MnGa experimental results have not been reported.

Another difference between the theory and the experiment is that the experiments are done with nonstoichiometric compositions. From the several effects of nonstoichiometry we consider here the change in the average number of valence electrons within a simple rigid band approximation. The eigenvalues from a calculation with a stoichiometric composition are used, but the summation in Eq. (1) is done with a varying band filling. The number of valence electrons is varied, and the Fermi level is determined in accordance with the new number of electrons. The results for the experimental structure are shown in Fig. 4 along with some experimental values for the MAE.

Already this simple approximation for the nonstoichiometry brings the theoretical MAE in good agreement with the experiment and reproduces correctly the experimental trend about the composition dependence of the MAE. The remaining discrepancies between calculated and experimental values of MAE could originate either from deficiencies of the used approximations such as the GGA or from experimental conditions such as the finite temperature, mentioned earlier, and other alloying effects.

Next, the MAE is used to calculate the magnetostriction coefficient of the cubic $L2_1$ structure. According to the linear magnetoelastic theory the MAE depends linearly on the tetragonal strain. The total energy can be written as a sum of magnetoelastic and elastic energy[32]:

$$E_{tot}=-\alpha B\epsilon+C\epsilon^2, \tag{2}$$

where ϵ is the tetragonal distortion, $\epsilon=2/3(c/a-1)$, $\alpha=1$ for magnetization parallel to tetragonal [001] axis, and $\alpha=-1/2$ for magnetization perpendicular to that axis, B is the magnetoelastic coupling constant and C is related to elastic constant C', $C=3V_0C'/2$, where V_0 is the volume of the unit cell. The magnetostriction coefficient λ_{001} is defined as the strain that minimizes the total energy of Eq. (2):

$$\lambda_{001}=-\frac{B}{2C}. \tag{3}$$

The linear variation of the MAE with the small distortions, Fig. 3, allows us to calculate the magnetostriction coefficient of the cubic $L2_1$ structure together with Eq. (3). The B constant is determined from the linear part of the MAE vs c/a plot and the elastic constant C' for the C coefficient is obtained either from calculations or experiments. The theoretical value for C' is 4.7 GPa (Ref. 33) while the experimental values vary from 4.5 GPa (Ref. 34) to 22 GPa (Ref. 35) According to the value used for C', the magnetostriction coefficient varies then from $\sim -500\times10^{-6}$ to $\sim -100\times10^{-6}$. The calculated magnetostriction coefficient has the same order of magnitude as the experimental one which is between $\sim -250\times10^{-6}$ and $\sim -130\times10^{-6}$ (Refs. 1 and 9) depending on the temperature and the composition. A direct comparison of theoretical and experimental magnetostriction is complicated because of the several sources for the differences: temperature, composition, the elastic constants, or the coefficient B. The calculations reproduce, however, the correct order of magnitude.

Because the number of the data points is not enough to describe the linear behavior of the MAE around $c/a=0.94$, Eq. (3) cannot be applied directly for the martensitic phase. However, some estimation of the magnetostriction coefficient in the martensitic phase can be done. The elastic constant C' of the tetragonal structure is 13.5 GPa,[33] and the slope of the MAE vs c/a curve near $c/a=0.94$ is around 3 times larger than near the cubic structure; see Fig. 3. Therefore the magnetostriction for the $c/a=0.94$ variant should be of the same order of magnitude as for the $L2_1$ structure. These findings confirm that the ordinary magnetostriction is a minor effect in the MSM shape change of 6%.

B. Microscopic origin of the MAE

Some qualitative information about the contribution of different atoms to the MAE can be obtained from the spin density. Because the total energy is a functional of the spin density, it is natural to assume that the spatial variation in the difference of spin density with different spin quantization axes gives information about the spatial contributions to the MAE. The spin density (the component parallel to the quantization axis) is calculated from the spin-orbit-perturbed wave functions and the resulting difference in the spin density between the [110] and [001] magnetization directions is shown in Fig. 5. It is interesting to note that for Ni the difference is positive and is mainly due to d_{z^2} orbitals, while for Mn the difference is negative and has mainly d_{xy} character. The directionality of the characters shows that the magnetic coupling is mainly between the atoms of the same species. The most important fact in Fig. 5 is that the spin density

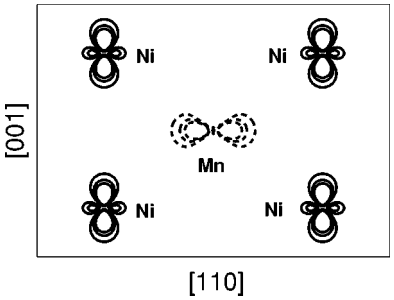

FIG. 5. Difference in spin density in $(1\bar{1}0)$ plane. Solid lines denote positive values with 10^{-3} $e/\text{Å}^3$ spacing between contours, dashed lines negative values with 10^{-4} $e/\text{Å}^3$ spacing.

difference for Ni is around an order of magnitude larger than for Mn. This suggests that the largest contribution to the MAE comes from Ni.

More information about the importance of the constituent atoms for the MAE can be obtained from the orbital moments. Both the OMA and the MAE originate from the spin-orbit coupling so that a large OMA is indicative of a large MAE in many cases. The orbital moments, which are $\sim 0.025\mu_B$ within the Ni spheres and $\sim 0.016\mu_B$ within the Mn spheres, are calculated using the spin-orbit-perturbed wave functions. The resulting total and atomic-sphere-decomposed OMA's are shown in Fig. 6 as a function of the distortion. It is seen that the OMA within the Ni sphere is about 2 times larger than in the Mn sphere. The shape of the curve is similar to the MAE as seen in Fig. 3, suggesting that the two quantities are related also in Ni_2MnGa. In other words, the atomic-sphere-decomposed OMA reinforces the argument that Ni has a larger contribution to the MAE than Mn, in accordance with the spin density.

The above considerations about the relationship between the MAE and the OMA can be put in a more quantitative form using arguments from second-order perturbation theory. In the cases with a single atom per unit cell the MAE ΔE and the OMA $\Delta\mu$ can be written as[19]

$$\Delta E = -\xi^2[a^{\uparrow\uparrow} + a^{\downarrow\downarrow} - a^{\uparrow\downarrow} - a^{\downarrow\uparrow}] \tag{4}$$

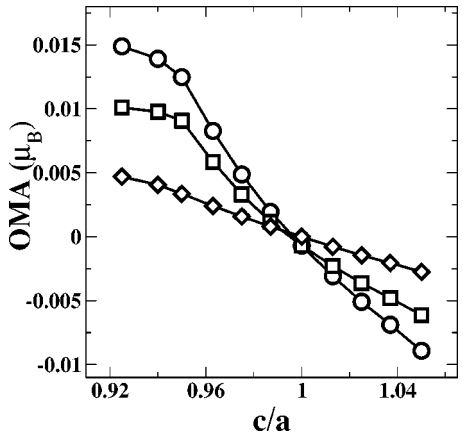

FIG. 6. The OMA as a function of the tetragonal distortion. (○) total, (□) Ni, and (◇) Mn.

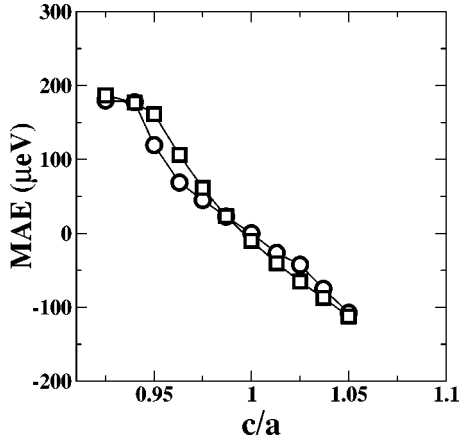

FIG. 7. MAE calculated with (○) force theorem, with (□) Eq. (8).

and

$$\Delta\mu = -4\xi[a^{\uparrow\uparrow} - a^{\downarrow\downarrow}]. \tag{5}$$

The $a^{\sigma_1\sigma_2}$ indicate the terms coming from the couplings between different spins. When spin flips are neglected and the majority band is assumed to be completely filled ($a^{\downarrow\downarrow} = a^{\uparrow\downarrow} = a^{\downarrow\uparrow} = 0$) these equations reduce to the linear relationship between the MAE and the OMA as shown earlier in Ref. 18. The above expressions can be further generalized to the case with several atoms in the unit cell[20]:

$$\Delta E = -\sum_q \xi_q^2[a_q^{\uparrow\uparrow} + a_q^{\downarrow\downarrow} - a_q^{\uparrow\downarrow} - a_q^{\downarrow\uparrow}] \tag{6}$$

and

$$\Delta\mu = -4\sum_q \xi_q[a_q^{\uparrow\uparrow} - a_q^{\downarrow\downarrow}]. \tag{7}$$

The relationship between the MAE and the OMA as given by Eqs. (6) and (7) is not necessarily linear even when spin flips and other spin sub bands are neglected because the spin-orbit coupling parameters ξ_q are different for different atoms.

Under the assumption that only the Ni and Mn contribute to the MAE and that spin flips and other spin subbands can be neglected, Eq. (6) can be written as

$$\Delta E = \frac{\xi_{\text{Ni}}}{4}\Delta\mu_{\text{Ni}} + \frac{\xi_{\text{Mn}}}{4}\Delta\mu_{\text{Mn}}. \tag{8}$$

Some estimates for the ξ_q can be obtained from an atomic program which gives $\xi_{\text{Ni}} \cong 121$ meV and $\xi_{\text{Mn}} \cong 60$ meV. If these values are used in Eq. (8), the resulting MAE's are larger than in Fig. 3. However, it is expected that in the crystalline alloy the ξ_q are reduced from their atomic values. A relatively good fit between the MAE calculated from Eq. (8) and the MAE calculated within the force theorem is obtained by using $\xi_{\text{Ni}} = 60$ meV and $\xi_{\text{Mn}} = 30$ meV as seen in Fig. 7. Together with the atomic-sphere-decomposed OMA (see Fig. 6) this suggests that Ni contributes to the MAE 4 times more than Mn. Although these fitted values for ξ_q may be an underestimation due to the neglect of the other spin

sub-band in Eq. (6), the importance of the Ni for the MAE is well established. This observation is quite surprising because the largest contribution for the magnetic moment comes from Mn. Altogether, it is seen that different magnetic properties originate from different atoms.

IV. CONCLUSIONS

The purpose of this research was to study the magnetic properties of Ni_2MnGa, which is an example of a magnetic shape-memory alloy. We assume that the relevant quantity for the MSM effect is the magnetic anisotropy energy. The MAE is studied with density-functional calculations to obtain insight into its distortion dependence and origins. Here, the MAE is found to vary linearly with small tetragonal distortions. Clearly, our calculations reproduce the experimental easy axis, which changes from [001] to [110] when changing the tetragonality from $c/a<1$ to $c/a>1$. In addition, the magnetostriction coefficient of the cubic $L2_1$ structure is determined to be in good agreement with the experiments. The magnetostriction in the martensitic phase is estimated to have the same order of magnitude as in the $L2_1$, corroborating the result that ordinary magnetostriction is a minor effect in the MSM phenomenon.

Although the theoretical MAE is close to the experimental values, we believe that a better fit can be obtained when the composition dependence is taken into account. We have accomplished that with a simple rigid band model, which shows that the MAE decreases about 50% with a small change in the composition, consistent with the experimental trend.

Microscopic origins of the MAE are studied first with the difference in the spin density for the two magnetization directions. This shows the orbital characters of the magnetic coupling and that the coupling is mainly between atoms of same species. The main finding of the current study is seen also in the spin density: Ni is more important for the MAE than Mn, and the role of Ga is negligible. More quantitative information about the importance of the constituent atoms for the MAE is obtained from the OMA. Detailed analysis of the relationship between the MAE and the OMA allows us to express the contribution of an atom to the MAE in terms of its OMA. The calculated OMA's show that the MAE results from Ni and Mn, and that about 80% of the MAE comes from Ni. Interesting in this result is that the situation is opposite for the magnetic moment, with $\sim 80\%$ of the magnetic moment coming from Mn.

The results presented show that the calculation of the MAE is feasible also in ternary compounds. Furthermore, we have shown how the OMA can be used in analyzing the importance of the constituent atoms. Our calculated MAE clarifies the origin of MAE expressions which could be used as input for higher level models, such as micromagnetic models. In view of these model calculations, more first-principles calculations could be performed: for example, the calculation of angular variation of the MAE or the OMA in orthorhombic structures would be interesting. On the other hand, as the MAE is important for the MSM effect, these calculations suggest further ideas how the Ni-Mn-Ga alloys should be optimized in order to maximize the MAE. We note that Ni has the largest contribution to the MAE, but on the other hand the MAE is sensitive to the band filling.

ACKNOWLEDGMENTS

This work has been supported by the Academy of Finland (Centers of Excellence Program 2000-2005) and by the National Technology Agency of Finland (TEKES) and the consortium of Finnish companies (ABB Corporate Research Oy, AdaptaMat Oy, Metso Oyj, Outokumpu Research Oy). A.A. is supported by the EU TMR program (Contract No. ERB4001GT954586). Computer facilities of the Center for Scientific Computing (CSC) Finland are greatly acknowledged. L.N. acknowledges support from the Swedish Research Council and the Swedish Foundation for Strategic Research.

*Electronic address: jen@fyslab.hut.fi

[1] K. Ullakko, J.K. Huang, C. Kantner, and R.C. O'Handley, Appl. Phys. Lett. **69**, 1966 (1996).

[2] *Shape Memory Alloys*, edited by H. Funakubo (Gordon and Breach, London, 1987).

[3] A.E. Clark, in *Ferromagnetic Materials*, edited by E. P. Wohlfarth (North-Holland, Amsterdam, 1980), Vol. 1, p. 531.

[4] S.J. Murray, M. Marioni, S.M. Allen, R.C. O'Handley, and T.A. Lograsso, Appl. Phys. Lett. **77**, 886 (2000).

[5] R.J. James and K.F. Hane, Acta Mater. **48**, 197 (2000).

[6] P.J. Webster, Contemp. Phys. **10**, 559 (1969).

[7] P.J. Webster, K.R.A. Ziebeck, S.L. Town, and M.S. Peak, Philos. Mag. B **49**, 295 (1984).

[8] A. Ayuela, J. Enkovaara, K. Ullakko, and R.M. Nieminen, J. Phys.: Condens. Matter **11**, 2017 (1999).

[9] R. Tickle and R.D. James, J. Magn. Magn. Mater. **195**, 627 (1999).

[10] S. Wirth, A. Leithe-Jasper, A.N. Vasil'ev, and J.M.D. Coey, J. Magn. Magn. Mater. **167**, L7 (1997).

[11] O. Heczko, K. Jurek, and K. Ullakko, J. Magn. Magn. Mater. **226**, 996 (2001).

[12] O. Heczko (private communication).

[13] The dipole-dipole anisotropy is estimated to be ~ -5 μeV per formula unit for the structure with $c/a=0.94$, so only the spin-orbit anisotropy is considered here.

[14] J. Trygg, B. Johansson, O. Eriksson, and J.M. Wills, Phys. Rev. Lett. **75**, 2871 (1995).

[15] O. Hjortstam, K. Baberschke, J.M. Wills, B. Johansson, and O. Eriksson, Phys. Rev. B **55**, 15 026 (1997).

[16] R. Wu and A.J. Freeman, J. Magn. Magn. Mater. **200**, 498 (1999).

[17] I. Galanakis, M. Alouani, and H. Dreyssé, Phys. Rev. B **62**, 6475 (2000).

[18] P. Bruno, Phys. Rev. B **39**, 865 (1989).

[19] G. van der Laan, J. Phys.: Condens. Matter **10**, 3239 (1998).

[20] P. James, Ph.D. thesis, Uppsala University, 1999.

[21] E. Wimmer, H. Krakauer, M. Weinert, and A.J. Freeman, Phys. Rev. B **24**, 864 (1981); M. Weinert, E. Wimmer, and A.J. Freeman, *ibid.* **26**, 4571 (1982), and references therein.

[22] P. Blaha, K. Schwarz, and J. Luitz, computger code WIEN 97, Vienna University of Technology, 1997 [improved and updated Unix version of the copyrighted WIEN code, which was published by P. Blaha, K. Schwarz, P. Sorantin, and S. B. Trickey, Comput. Phys. Commun. **59**, 399 (1990)].
[23] J.P. Perdew, K. Burke, and M. Ernzerhof, Phys. Rev. Lett. **77**, 3865 (1996).
[24] A.H. MacDonald, W.E. Pickett, and D.D. Koelling, J. Phys. C **13**, 2675 (1980).
[25] A.R. Mackintosh and O.K. Andersen, in *Electrons at the Fermi Surface*, edited by M. Springford (Cambridge University Press, Cambridge, England, 1980).
[26] M. Weinert, R.E. Watson, and J.W. Davenport, Phys. Rev. B **32**, 2115 (1985).
[27] C.-L. Fu and K.M. Ho, Phys. Rev. B **28**, 5480 (1983).
[28] A. de Vita and M.J. Gillan, J. Phys.: Condens. Matter **3**, 6225 (1991).
[29] O. Jepsen and O.K. Andersen, Solid State Commun. **9**, 1763 (1971).
[30] P.E. Blöchl, O. Jepsen, and O.K. Andersen, Phys. Rev. B **49**, 16 223 (1994).
[31] A. Sozinov, A.A. Likhachev, and K. Ullakko, Proc. SPIE **4333**, 189 (2001).
[32] P. James, O. Eriksson, O. Hjortstam, B. Johansson, and L. Nordström, Appl. Phys. Lett. **76**, 915 (2000).
[33] A. Ayuela, J. Enkovaara, and R.M. Nieminen (unpublished).
[34] J. Worgull, E. Petti, and J. Trivisonno, Phys. Rev. B **54**, 15 695 (1996).
[35] L. Mañosa, A. González-Comas, E. Obradó, A. Planes, V.A. Chernenko, V.V. Kokorin, and E. Cesari, Phys. Rev. B **55**, 11 068 (1997).